Hydrodynamic Behaviors of the Two-Phase Turbulent Flow of Microalgae Suspension and CO_2 in a Photobioreactor for Biofuel Production

MOHAMMAD IFTEKHAR MONIR[1,2,*], NURUN NAHAR[3], UJJWAL KUMAR DEB[3], ANJAN KUMAR CHOWDHURY[2]

[1]Department of Mathematics,
Premier University, Chattogram,
BANGLADESH

[2]Jamal Nazrul Islam Research Center for Mathematical and Physical Sciences,
University of Chittagong,
BANGLADESH

[3]Department of Mathematics,
Chittagong University of Engineering and Technology,
BANGLADESH

**Corresponding Author*

Abstract: - Microalgae cultivation in horizontal loop tubular photobioreactors (HLTPs) is more efficient for biofuel production than other methods. It is important to inject CO_2 into the photobioreactors to ensure microalgal growth. Due to the complex flow path and bubble arising from CO_2 penetration in the tube, turbulence may occur in the flow. In this work, a two-phase turbulent flow of CO_2 and microalgae suspension is considered for simulating the flow. An HLTP is used here as the computational domain for our simulation. Besides a slow growth in the culture, we have observed that the flow inside the reactor forms a parabolic shape at the straight portion. However, a wavering flow is found around the U-loop portion of the tube. The pressure is gradually dropped along the arc length. The shear rate is somewhat high and fluctuates within the tube. The effect of the nutrient on growth is also found.

Key-Words: - Biofuel, Finite Element Method, Two-phase flow, Photobioreactor, Simulation, Microalgae.

Received: July 17, 2025. Revised: November 14, 2025. Accepted: December 11, 2025. Published: June 2, 2026.

1 Introduction

In most cases, the environment is hampered by using petroleum-based fuels due to increasing Green House Gases (GHG), like CO_2, CO, etc. Moreover, this fuel type is now predicted as unsustainable because of decreasing supplies. The impact of GHG is not only the cause of Global Warming (GW) but also has a negative influence on the total environment and individual life. In this situation, carbon-neutral and renewable fuels are essential for both economic and environmental sustainability, [1]. The potential of plant-based biofuels as a sustainable and carbon-neutral alternative to petroleum fuels is impressive, [2]. Although biofuels can be produced from Corn, Soybean, Canola, Jatropha, Coconut, Palm, Microalgae, etc., the more promising ones are microalgae, [3]. Several microalgae species are ideal biomass sources for biofuel technology due to their large productivity and lower greenhouse gas secretion capability, [1], [4]. In the algae production sector, there are two main systems: the open pond system and the closed bioreactor system. Since open ponds are inexpensive to operate, algae have historically been grown there for extended periods. However, due to biological and technical constraints on controlling growth conditions and contamination threats, closed photobioreactor (PBR) systems have to be developed. Besides prevention of contamination with other micro-organisms in closed systems, the biomass recovery cost is lower than that in the open ponds, [1], [5], [6]. The Tubular PBRs are the best category among the different PBR designs for producing biomass outdoors, [3], [7], [8], [9]. In this culturing technique, different factors such as Light, Temperature, CO_2, mass transfer, turbulence, and liquid circulation time have a direct influence on microalgae growth. In the process of cultivating microalgae, CO_2 gas must be injected into the tubular reactor; however, this gas causes bubbles inside the PBR, which alter the flow patterns. Useful algae production practices and the PBR model still do not work as expected due to inadequate knowledge of turbulent flow behavior in the reactor. We examine a two-phase turbulent flow of microalgae suspension and CO_2 in this work to comprehend fluid dynamics phenomena that arise from the injection of CO_2 gas into a Horizontal Loop Tubular Photobioreactor (HLTP). Our goal is to study the pressure and shear stress inside the HLTP to gain an in-depth understanding of flow phenomena to increase cell growth.

2 Literature Review and Theoretical Framework

Two-phase flows can be found in many different industrial applications as well as in nature. A two-phase fluid is typically referred to as a mixture, [10]. Different kinds of two-phase flows can be produced by combining two different phases, such as gas and liquid, liquid and solid, liquid and liquid, and so forth. A two-phase gas-liquid flow of CO_2 and microalgae suspension is taken into consideration in this work. Various studies have been done on single-phase as well as two-phase flows. A computational model for an incompressible, laminar, and Newtonian single-phase microalgae suspension flow in a single-loop tubular reactor was used to simulate and identify the sensitive region in the reactor that might cause cell fragility, which reduces the optimization of the biofuel production, [11]. The growth of microalgae in a photobioreactor was calculated using a computational growth model that was related to the average irradiance and the results demonstrated that the growth of microalgae varied with the average irradiance over a year, [12]. A two-phase incompressible and laminar flow of oil and water in a typical circular tube domain was analyzed using a computational fluid dynamics (CFD) model at various times. The flow dynamics, comprising the velocity profile, volume fraction, shear rate, pressure distributions, and interfacial thicknesses, were analyzed using the model, [13]. Understanding fluid dynamics phenomena after injecting CO_2 gas into a tubular photobioreactor (PBR) through a two-phase incompressible and laminar flow of CO_2 and microalgae suspension revealed that the U-loop area is responsible for cell fragility, [14]. Now for evaluating the flow behaviors in case of a two-phase turbulent flow of microalgae suspension and CO_2 gas in the tubular photobioreactor, a higher concentration is needed to provide. Consequently, the flow becomes turbulent.

The morphology of microalgae shows that the cell membrane of matured microalgae becomes very thin. As a result, cells become shear-sensitive from a mathematical point of view. One of the challenging tasks in the algae cultivation process is the development of a mathematical model that helps in an in-depth understanding of flow patterns inside the reactor. In this study, our main goal is to predict the microalgae suspension flow phenomena at different cross sections inside the reactor using the simulation process. Without understanding the flow dynamics, it is tough to make a decision about the cell damage area of the reactor geometry. Once identify the sensitive area, we can take action to prevent cell damage by controlling the initial conditions. The approximate behavior of the system can be found by using a computational model. Approximate solution methods are more popular than direct integration methods. With the arrival of high-speed computers, the Finite Element Method (FEM) is the most appropriate method for obtaining approximate solutions with high accuracy, [15]. The ability to handle complex geometries using irregular grids of varied forms and to provide a collection of functions that indicate the distinction of differential equations between grid points makes the finite element method superior to other approaches for the desired approximation, [16]. So, the finite element approximation method is applied to analyze the microalgae suspension flow inside the reactor. Some relevant studies are available in [17], [18].

3 Methodology

3.1 Computational Domain and Mesh Design

This work uses an airlift-driven, single-loop horizontal tubular photobioreactor as the computational domain. Figure 1 depicts a typical circular tube domain and its mesh design with 6.4 m in length and 0.025 m in radius. The domain's surface area and working volume are 1.005 m^2 and 0.01257 m^3, respectively. The result for the mesh with 60587 elements is significant compared to the mesh with 51014 elements, and further refinement with 82863 elements does not significantly change the outcome (Figure 2). Since the mesh design greatly influences the accuracy of the numerical findings, we thought that the mesh design with 60587 elements would be an appropriate choice for our simulation. Minimum quality: 0.1371, average quality: 0.5719, domains: 3, faces: 20, edges: 36, points: 20, and 619,748 degrees of freedom. Figure 2 depicts the grid sensitivity analysis for validation. Inside the HLTP, a uniform mixture of CO_2 and microalgae suspension is injected. It is assumed that the flow pattern of this mixture is turbulent, and also assumed that it is an incompressible two-phase Newtonian fluid.

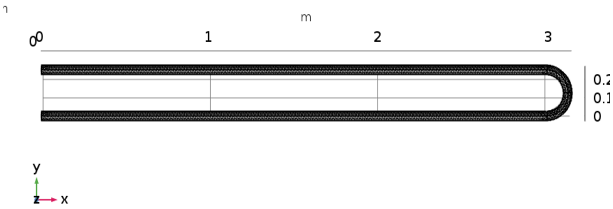

Fig. 1: Computational Domain and its Mesh Design
Source: created by the authors

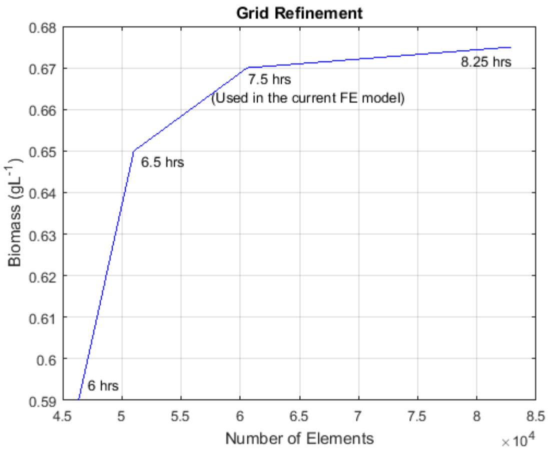

Fig. 2: Grid sensitivity analysis
Source: created by the author

3.2 Experimental Setup

A photobioreactor controlled by an airlift system [19], including a continuous tubular solar receiver, comprises two primary components: the airlift mechanism and the looping solar receiver (Figure 3). The purpose of the airlift machine is to move the culture via the solar receiver. Gas bubbles are kept from recirculating into the solar loop by a gas-liquid separator in the upper section of the airlift column. Oxygen builds up during photosynthesis in the solar tube and is removed in the airlift zone as the fluid exits the solar loop. The pertinent design elements are then covered, one for each of the two zones.

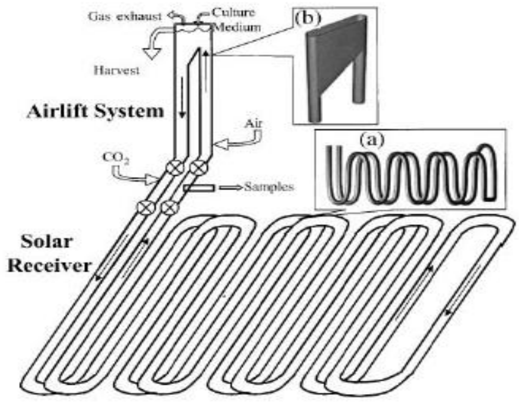

Fig. 3: The outdoor culture system with details of the solar loop (a) and the degasser zone (b)
Source: created by the authors

3.3 Governing Equations

Current flow behavior is expressed by using the following most widely used set of equations for incompressible fluid dynamics:
Continuity equation, which is the mass conservation equation:

$$\nabla \cdot \mathbf{u} = 0 \tag{1}$$

where **u** is the velocity field.

The Navier-Stokes equation, which is the equation of motion:

$$\rho \frac{\partial \boldsymbol{u}}{\partial t} + \rho(\mathbf{u} \cdot \boldsymbol{\nabla})\mathbf{u} = \boldsymbol{\nabla} \cdot [p\boldsymbol{I} + (\mu + \mu_T)(\nabla u + (\nabla u)^T] + \rho \boldsymbol{g} + F_{st} + F \tag{2}$$

where ρ is the density, p is the pressure, μ is the dynamic viscosity, $\mathbf{F}_{st}$ is the surface tension force acting at the gas/liquid interface, and **F** is the body force. The k–ϵ turbulence model is given by the equations:

$$\rho \frac{\partial k}{\partial t} + \rho(\mathbf{u} \cdot \boldsymbol{\nabla})k = \nabla \cdot \left[\left(\mu + \frac{\mu_T}{\sigma_k}\right)\nabla k\right] + P_k - \rho\epsilon \tag{3}$$

$$\rho \frac{\partial \epsilon}{\partial t} + \rho(\mathbf{u} \cdot \boldsymbol{\nabla})k = \nabla \cdot \left[\left(\mu + \frac{\mu_T}{\sigma_\epsilon}\right)\nabla \epsilon\right] + C_{\epsilon 1}\frac{\epsilon}{k}P_k - C_{\epsilon 2}\rho\frac{\epsilon^2}{k} \tag{4}$$

where, $\mu_T = \rho C_\mu \frac{k^2}{\epsilon}$

$$P_k = \mu_T[\nabla \mathbf{u}: (\nabla \mathbf{u} + (\boldsymbol{\nabla}\mathbf{u})^T)]$$

Interfacing of two phases is described by the equation:

$$\frac{\partial \emptyset}{\partial t} + \mathbf{u} \cdot \boldsymbol{\nabla}\emptyset = \gamma \nabla \cdot \left(\epsilon_{ls}\nabla\emptyset - \emptyset(1 - \emptyset)\frac{\nabla\emptyset}{|\nabla\emptyset|}\right) \tag{5}$$

where the ϵ determines the thickness of the interface, ϕ is the level set function, k is the turbulence kinetic energy, and γ is the intensity of reinitialization. Wall functions are:

$$\mathbf{u}_{rel} \cdot \mathbf{n} = 0 \quad (6)$$

$$[(\mu + \mu_T)(\nabla\mathbf{u} + (\nabla\mathbf{u})^T)]\mathbf{n} = -\rho \frac{U_\tau}{\delta_w^+}\mathbf{u}_{rel\cdot tang} \quad (7)$$

where, $\mathbf{u_{rel}} = \mathbf{u} - \mathbf{u}_{\text{w}\cdot\text{proj}}$, $\mathbf{u}_{\text{w}\cdot\text{proj}} = \frac{\mathbf{u}_\text{w} - (\mathbf{u}_w\cdot\mathbf{n})\mathbf{n}}{\|\boldsymbol{u}_w - (\boldsymbol{u}_w\cdot\boldsymbol{n})\boldsymbol{n}\|} \cdot \|\mathbf{u}_w\|$

$$\mathbf{u}_{rel\cdot tang} = \mathbf{u}_{rel} - (\mathbf{u}_{rel}\cdot\mathbf{n})\mathbf{n}$$

$$\boldsymbol{\nabla}k \cdot \mathbf{n} = 0,\ \epsilon = -\rho\frac{C_\mu k^2}{k_v \delta_w^+ \mu}$$

At the inlet $\mathbf{u} = \mathbf{u}_0$, $k = \frac{3}{2}(\frac{\|\mathbf{u}_0\|}{T})^2$, $\epsilon = C_\mu^{3/4}\frac{k^{3/2}}{L_2}$, $\emptyset = V_f$

And at the outlet: $[-pI + (\mu + \mu_T)(\nabla\mathbf{u} + (\nabla\mathbf{u})^T]\mathbf{n} = -f_0\mathbf{n}$
$\nabla k \cdot \mathbf{n} = 0$, $\nabla\epsilon \cdot \mathbf{n} = 0$

3.4 Finite Element Approximation

Variational statement:

$$r(x,t) = \rho\left(\frac{\partial\mathbf{u}}{\partial x} + \mathbf{u}\cdot\nabla\mathbf{u}\right) - \nabla\cdot[pI + (\mu + \mu_T)(\nabla\mathbf{u} + (\boldsymbol{\nabla}\mathbf{u})^T)] - \rho\boldsymbol{g} - \boldsymbol{F_{st}} \quad (8)$$

According to the weighted residual method [15], there is $(\mathbf{u}, p) \in \mathbf{V} \times Q$ such that for every $t \in \mathbf{I}$

$$(\mathbf{r}, v) = 0,\ \forall v \in V \text{ and } v = 0 \text{ on } \Gamma_u \quad (9)$$

$$(\nabla\cdot\mathbf{u}, q) = 0, \quad \forall q \in Q \quad (10)$$

$$\mathbf{u}(x, 0) = \mathbf{u}_0 \quad \text{in } \Omega \quad (11)$$

$$\mathbf{u}(x, t) = \bar{\mathbf{u}} \quad \forall x \in \Gamma_u \quad (12)$$

where V and Q are velocity and pressure spaces, and the inner product is defined by

$$(\mathrm{a}, \mathrm{b}) = \int_\Omega \mathbf{a}\cdot\mathbf{b}\, d\Omega \quad (13)$$

The integral representation of (9) is presented as follows:

$$\int_\Omega \frac{D\mathbf{u}}{Dt}\cdot\mathbf{v}\, d\Omega + \int_\Omega([p\mathbf{I} + (\mu + \mu_T)(\nabla\mathbf{u} + (\nabla\mathbf{u})^T)]\nabla\mathbf{v})\, d\Omega - \int_\Omega \rho\mathbf{g}\cdot\mathbf{v}\, d\Omega - \int_\Omega \mathbf{F}_{st}\cdot\mathbf{v}\, d\Omega - \int_\Omega \mathbf{F}\cdot\mathbf{v}\, d\Omega = \int_{\partial\Omega}\bar{\mathbf{T}}\cdot\mathbf{v}\, ds \quad (14)$$

We consider a bounded and connected computational domain Ω with boundary $\partial\Omega = \Gamma_u \cup \Gamma_t$, where $\Gamma_u \cup \Gamma_t = \emptyset$. On Γ_u, the movement u is prescribed, and on Γ_t, the surface traction t is prescribed, v is chosen to be zero on Γ_u.

The variational statement of the problem is, Find $(\mathbf{u}, p) \in \mathbf{V} \times Q$ such that for every $t \in \mathbf{I}$

$$\left(\rho\frac{Du}{Dt}, v\right) + [pI + [(\mu + \mu_T)(\nabla u + (\nabla u)^T)], \nabla u] - (\rho g, v) - (F_{st}, v) - (F, v) = b(\bar{T}, v), \forall v \in V_0 \quad (15)$$

$$(\nabla\cdot\mathbf{u}, q) = 0, \forall q \in Q \quad (16)$$

$$u(x, 0) = u_0 \ in\ \Omega \quad (17)$$

$$u = \bar{u} \ on\ \Gamma_\text{u} \quad (18)$$

$$V = \{v | v \in [H^1(\Omega)]^2\} \quad (19)$$

$$V_0 = \{v | v \in V \ and\ v = 0 \ on\ \Gamma_\text{u}\} \quad (20)$$

$$Q = \{\beta | \beta \in H^1(\Omega)\} \quad (21)$$

This variational statement is commonly referred to as the weak formulation of a Newtonian incompressible flow in two phases within a computational domain **Ω**.

3.4.1 Galerkin Approximation

To find the Finite Element approximation, let $V_h \subset V$ be an N-dimensional subspace of V with basis functions $\{\phi_1, \phi_2, \phi_3, \cdots, \phi_N\}$. Approximating v and q in equations (15–22) by

$v_h = \sum_{k=1}^N \emptyset_k v_k$ and $q = \sum_{P=1}^M \theta_p q_p$

$$\sum_{k=1}^N\{\left(\rho\frac{Du}{Dt}, \emptyset_k\right) + [(pI + [(\mu + \mu_T)(\nabla u + (\nabla u)^T)], \nabla\emptyset_k] - (\rho g, \emptyset_k) - (F_{st}, \emptyset_k) - (F, \emptyset_k) - b(\bar{T}, \emptyset_k)\}v_k = 0 \quad (22)$$

$$\sum_{p=1}^M(\nabla\cdot u,\ \theta_p)q_p = 0 \quad (23)$$

These can be written as

$$\left(\rho\frac{\partial u}{\partial t}, \emptyset_k\right) + (\rho\mathbf{u}\cdot\boldsymbol{\nabla}\mathbf{u}, \emptyset_k) + [(pI + [(\nabla u + (\nabla u)^T)], \nabla\emptyset_k] = \{(\rho g, \emptyset_k) + (F_{st}, \emptyset_k) + (F, \emptyset_k) + b(\bar{T}, \emptyset_k)\} \quad (24)$$

$$(\boldsymbol{\nabla}\cdot\mathbf{u}, \theta_p) = 0 \quad (25)$$

Now, approximating u and p respectively by $u_h = \sum_{l=1}^N \emptyset_l u_l$ and $p_h = \sum_{p=1}^M w_p p_p$

Therefore, we get from the equations (24) and (25)

$$\sum_{l=1}^N\{(\rho\emptyset_l, \emptyset_k)\dot{u}_l + (\rho\emptyset_l\cdot\nabla\emptyset_l, \emptyset_k)u_l + (\mu\nabla\emptyset_l, \nabla\emptyset_k)u_l + (\mu(\nabla\emptyset_l)^T, \nabla\emptyset_k)u_l^T + (\mu_T\nabla\emptyset_l, \nabla\emptyset_k)u_l + (\mu_T(\nabla\emptyset_l)^T, \nabla\emptyset_k)u_l^T + \sum_{p=1}^M(I_p, \nabla\emptyset_k)p_p = (\rho g, \emptyset_k) + (F_{st}, \emptyset_k) + (F, \emptyset_k) + b(\bar{T}, \emptyset_k) \quad (26)$$

$$\sum_{k=1}^N(\nabla\cdot\emptyset_k, I_p)u_k = 0 \quad (27)$$

According to the Galerkin method, the weighting functions are chosen to coincide with the basis functions. We seek an approximate solution such that the total weighting residual error over Ω vanishes.

Let u_k be the corresponding finite element solution using equation (27). Then there exists a constant c such that

$$\max_{t \in I} \|u(t) - u_k(t)\| \leq c\left(1 + \left|\log \frac{T}{h^2}\right|\right) \max_{t \in I} h^2 \|u(t)\|_{H^2(\boldsymbol{\Omega})}$$

where h is the minimum step size.

3.5 Growth Kinetics

The rate of photosynthesis is modeled as **[**20**]**:

$$P = P_m \frac{I}{I_k + I} \tag{28}$$

where the variables P, P_m, I, and I_k represent the specific rate of photosynthesis, maximum specific rate of photosynthesis, light intensity reaching the cells, and constant based on algal species, respectively. The rate of photosynthesis across the entire culture concerning the incident light intensity (I_0) that reaches the system's external surface. Using the Beer-Lambert law for light distribution in combination with a Monod-like function, the local rate of photosynthesis can be computed as follows, [20]:

$$P(l) = P_m \frac{I_0 e^{-\sigma x l}}{I_k + I_0 e^{-\sigma x l}} \tag{29}$$

where x is the cell concentration, I_k is a saturation constant, P_m is the maximum volumetric rate of photosynthesis, σ is the extinction coefficient indicating the broth's degree of light absorption, and $P(l)$ is the local volumetric rate of photosynthesis at a distance of l from the system's external boundary. After that, the rate of photosynthesis for the entire system P can be calculated by integrating $P(l)$ across the system volume in the following way, [20]:

$$P = \int_V P(l)\, dV \tag{30}$$

where dV is the volume of the discrete elements and V is the culture volume.

A modified version of the Monod equation called the Haldane equation is frequently used to explain how substrate inhibition affects the transient behavior of cells, [21], [22], [23]:

$$\mu = \mu_{max} \frac{S}{S + K_S + \frac{S^2}{K_{iS}}} \tag{31}$$

Here, the substrate concentration is S, the substrate saturation constant is K_S, the substrate inhibition constant is K_{iS}, and the specific growth rate is μ. The maximal specific growth rate is represented by μ_{max}. Nutrient deficiency is known to promote oil buildup while preventing biomass development, [24], [25]. Furthermore, light intensity is essential for microalgae proliferation and lipid accumulation, [26], [27].

Consequently, the Haldane equation (represented by equation (31)) must be improved to consider the extra effects of nutrient concentration and light intensity. Utilizing two distinct expressions for the N effect as a substrate, the specific (oil-free) biomass growth and the lipid accumulation rate were reported here [22]. This is because N affects biomass concentration and lipid buildup differently. The influence of light strength as a pseudo-substrate was also modeled using the Aiba model, [28], [29].

Therefore, μ_X, the specific oil-free biomass development rate, can be expressed as follows using a pseudo-triple substrate expression:

$$\mu_X = \mu_{Xmax} \frac{S}{S + K_{XS} + \frac{S^2}{K_{iXS}}} \cdot \frac{N}{N + K_{XN} + \frac{N^2}{K_{iXN}}} \cdot \frac{I(l)}{I(l) + K_{XI(l)} + \frac{I(l)^2}{K_{iXI(l)}}} \tag{32}$$

where μ_{Xmax}, the maximum specific growth rate of oil-free biomass on acetate substrate (hereafter referred to as a substrate), is determined by the concentration of nutrient N and the intensity of local light I (l). The saturation constants are K_{XS}, K_{XN}, and K_{XI}, and the inhibition constants for oil-free biomass growth are K_{iXS}, K_{iXN} and K_{iXI} depending on the substrate, nitrogen absorption, and light intensity, respectively. Finally, the microalgae growth rate is expressed as:

$$\frac{dX}{dt} = \mu_X X \tag{33}$$

Table 1. Physical properties of fluids

Property	Value
Density of microalgae suspension	$1020 kgm^{-3}$
Density of CO_2	$1.8 kgm^{-3}$
Inlet velocity	$0.5 ms^{-1}$
Turbulent intensity	0.05
Turbulence length scale	$0.01 m$

Source: created by the authors in simulation

Table 2. Parameters of the growth model

Name	Value
Maximum growth rate	$0.063[1/h]$
Substrate	$2.1[gL^{-1}]$
Nitrogen	$0.098[gL^{-1}]$
Maximum specific growth rate	$0.227[h^{-1}]$
Saturation constant based on substrate	$0.050[gSL^{-1}]$
Inhibition constant based on substrate	$9.923[gSL^{-1}]$
Saturation constant based on nutrients	$0.065[gNL^{-1}]$
Inhibition constant based on nutrients	$0.500[gNL^{-1}]$
Saturation constant based on intensity	$19.519[L^{-2}J]$
Inhibition constant based on intensity	$2053.924[L^{-2}J]$
Incident light Intensity	$125[L^{-2}J]$
Biomass concentration	$458.6[mgL^{-1}]$
Molar Extinction coefficient	$34.104[g(mgL^{-1})^{-1}Lm^{-1}]$

Source: [31]

4 Result and Discussion

In this study, the two-phase flows of CO_2 and microalgae suspension are simulated using COMSOL Multiphysics. Table 1 and Table 2 provide the parameters and properties of the fluid phases, respectively. We have examined the flow's shear rate distributions, pressure, and velocity magnitude. Besides the hydrodynamical behavior analysis of the flow, the biomass production scenario has also been observed. To validate our simulation setup, a comparison with experimental work regarding biomass production has been done, [30]. Experiments [30] were conducted for the investigation of the effect of each metabolite on biomass growth and on lipid accumulation. The model was validated for different sets of substrate concentrations. To observe the biomass growth condition, a simulation has been done with a two-phase turbulent flow of microalgae and CO_2 in a horizontal single-loop tubular photobioreactor including nitrogen as a nutrient. The mass flow pattern through the whole computational domain (Figure 4(a)) reflects the behavior of the flow in times at different cross sections of the tube. The longitudinal view of the flow is given in Figure 4(b). Figures 4(a) and 4(b) show the flow behavior across the entire computational domain at time t=200 hours. From the figures, we observe that the different cross-sectional views of the flow pattern and the almost similar flow pattern, where the maximum velocity is observed at the middle of the tube. From the legend, it is clear that the flow in the middle is almost double compared to the wall. At the wall, the velocity is approximately zero due to the no-slip condition.

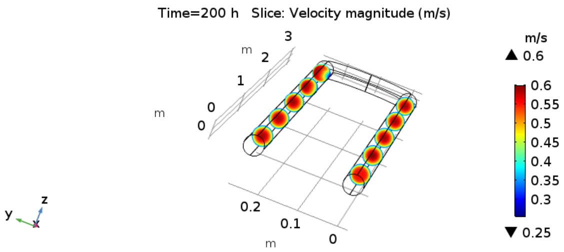

Fig. 4(a): Velocity profile of the microalgae culture through the domain of the reactor (cross-sectional view)
Source: created by the authors

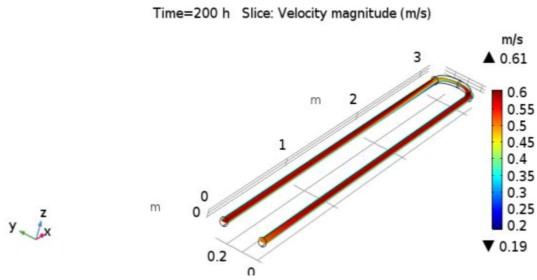

Fig. 4(b): Velocity profile of the microalgae culture through the domain of the reactor (longitudinal view)
Source: created by the authors

The parabolic shape of the flow (Figure 5) validates the setup of the simulation. The highest velocity at the center of the tube and the lowest velocity at the wall of the tube acknowledge the appropriate application of the no-slip condition. The velocity magnitude has gradually increased from the lower part of the tube and reached a maximum at the middle, which is around 0.6m/s, and again gradually decreased to about zero due to the no-slip condition at the wall. A regular pressure drop is found from the inlet to the outlet except at the U-loop portion of the tube (Figure 6). Around the U-loop, we found a sharp fall of around 100 Pa. Sudden pressure fluctuations are observed at the entrance and exit of the U-loop portion. These fluctuations may result from fittings and bends. Pressure and flow inside the system are directly correlated. This means that the flow rates were gradually decreasing from inlet to outlet, whereas the flow becomes wavering in nature at the edge of the u-loop portion.

The rate at which a material deforms across a neighboring layer due to velocity gradient is known as the shear rate. Measured in reciprocal seconds, the flow rate and the vessel cross-section both affect the shear rate. Figure 7 shows that at the center of the reactor, the shear rate is about zero, which means that almost no deformation in the shape of the elements occurred at the center of the tube, but Figure 8 shows that near the wall of the tube, the deformation rate of the elements is significant.

The numerical representation of the degree of turbulence in a certain flow is called turbulent kinetic energy. The flow velocity fluctuation's root mean square can be used to quantify it. The mean kinetic energy per unit mass for a turbulent flow is the simplest definition of it in fluid dynamics. Figure 9 shows the turbulent kinetic energy of the flow near the wall of the tube. It is viewed that at the entrance of the U-loop, the kinetic energy fluctuates due to the geometry of the tube. After crossing the loop, it has a logistic shape of growth of energy to reform the shape of the flow.

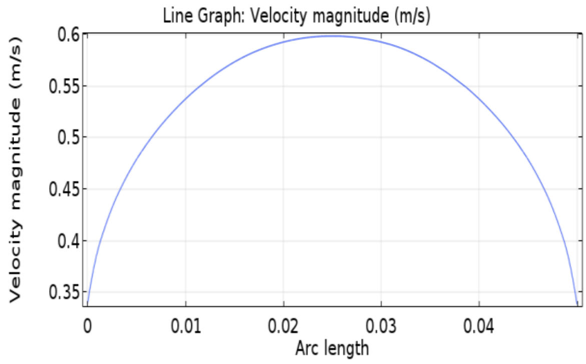

Fig. 5: Velocity magnitude of the flow on the vertical cross-section at x=0.8m
Source: created by the authors

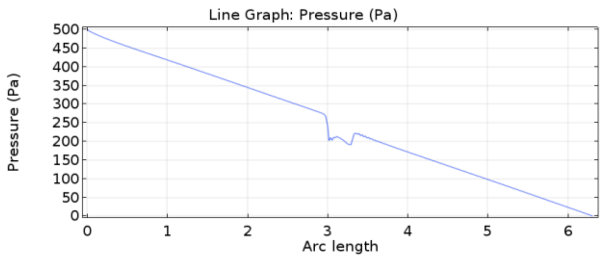

Fig. 6: Pressure distribution on the wall of the domain.
Source: created by the authors

The microalgae cell growth is represented in this model using the increase in the amount of biomass concentration. At low nutrient levels, turbulence can simplify nutrient transfer to algal cells, facilitate the nutrient intake rate, and hence enhance the growth rates, [32]. Figure 10 shows the comparison for validation between the present model result of biomass concentration for the total time at the point $x = 2.5m$ in the inlet side of the tube and the experimental result, [30]. A good agreement is remarked for the simulation and experimental results.

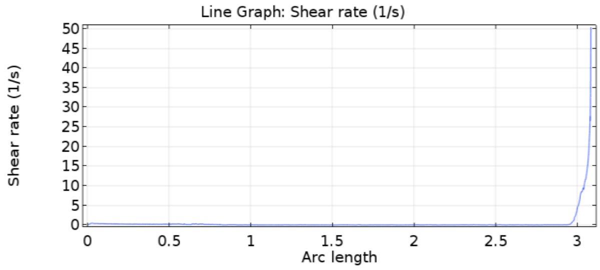

Fig. 7: Shear rate distribution at the center of the inlet side of the tubular reactor at the time t=200h
Source: created by the authors

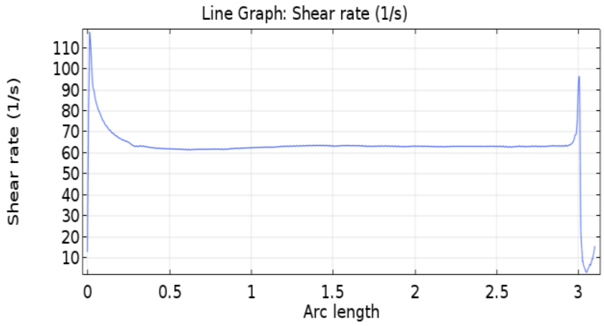

Fig. 8: Shear rate distribution on the wall of the inlet side of the tube
Source: created by the authors

The cell concentration forms a logistic curve for both cases. A very slow growth is observed in the initial phase. Later, the cell concentration is noted exponentially and eventually reaches the saturation level. The scenario is significantly matched with the experimental result, [30].

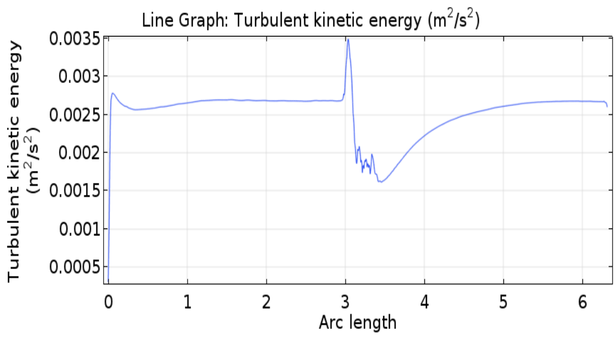

Fig. 9: Turbulent kinetic energy along the domain
Source: created by the authors

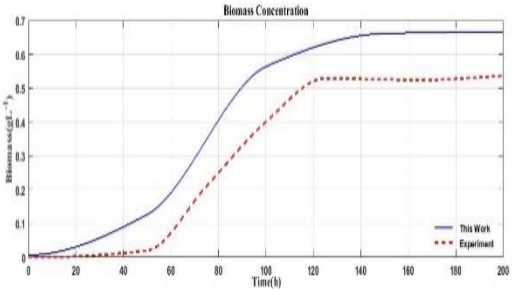

Fig. 10: Comparison of biomass concentration between simulation and experimental results.
Source: created by the authors

5 Conclusion

A computational model has been designed to observe the flow behavior of a two-phase turbulent flow of microalgae suspension and CO_2. Besides, the nutrient effect is also taken into account for measuring the growth. A perfect parabolic shape of velocity due to the flow is seen inside the reactor. To observe the reasons of variation in velocity, the pressure distribution has been studied. Comparative velocity among elements has been studied by means of shear rate. Fluid elements become shear sensitive near the wall and at U-loop portion of the tube. To overlook the intensity of turbulence in the flow, the behavior 'turbulence kinetic energy' is extracted. Due to complex geometrical shape, kinetic energy fluctuations are executed in the U-loop portion of the tube. For validation, the performance of growth model is compared with an experimental work which shows a good consistency. Finally, it can be claimed that the computational model worked as expected. Understanding the dynamics of cell production makes it very logical to move towards for a large-scale production. Since wavering flow exits in the U-loop portion of the tube, it is important to control the initial conditions as well as fix up the appropriate inner and outer radii of the tube to make the flow quieter and to reduce the cell fragility at the U-loop portion.

Acknowledgements:
The authors are grateful to The Centre of excellence in Mathematics, Department of Mathematics, Mahidol University, Bangkok, Thailand and Simulation Lab, Department of Mathematics, Chittagong University of Engineering and Technology, Chattogram, Bangladesh for technical support in this research.

References:

[1] Y. Chisti, "Biodiesel from microalgae", *Biotechnology Advances*, vol. 25, 2007, pp. 294-306. https://doi.org/10.1016/j.biotechadv.2007.02.001.

[2] V. H. Smith, B. S. M. Sturm, F. J. deNoyelles and S. A. Billings, "The ecology of algal biodiesel production", *Trends in ecology and evolution*, vol. 25, no. 5, 2010, pp. 301–309. https://doi.org/10.1016/j.tree.2009.11.007.

[3] T. M. Mata, A. A. Martins and N. S. Caetano, "Microalgae for biodiesel production and other applications: A review", *Renewable and Sustainable Energy Reviews*, vol. 14, 2010, no. 1, pp. 217–232. https://doi.org/10.1016/j.rser.2009.07.020.

[4] Y. Chisti, "Biodiesel from microalgae beats bioethanol", *Trends in Biotechnology*, vol. 26, 2008, no. 3, pp. 126–131. https://doi.org/10.1016/j.tibtech.2007.12.002.

[5] M. C. Flickinger and S. W. Drew (eds.), "*Encyclopedia of Bioprocess Technology: Fermentation, Biocatalysis, and Bioseparation*", Wiley, New York, 1999.

[6] M. R. Tredici, G. C. Zittelli and L. Rodolfi, "*Photobioreactors. Encyclopedia of industrial biotechnology: bioprocess, bioseparation, and cell technology*", pp. 1–15, 2009.

[7] L. B. Wu, Z, Li, and Y. Z. Song, "Numerical investigation of flow characteristics and irradiance history in a novel photobioreactor", *African Journal of Biotechnology*, vol. 8, 2009, no. 18, pp. 4672–4679, [Online]. https://academicjournals.org/journal/AJB/article-abstract/1EB4BCE9350 (Accessed Date: October 10, 2025).

[8] C. U. Ugwu, H. Aoyagi and H. Uchiyama, "Photobioreactors for mass cultivation of algae", *Bioresource Technology*, vol. 99, 2008, pp. 4021–4028. https://doi.org/10.1016/j.biortech.2007.01.046.

[9] O. Pulz, "Photobioreactors: production systems for phototrophic microorganisms." *Appl Microbiol Biotechnol*, vol. 57, 2001, no. 3, pp. 287–293. https://doi.org/10.1007/s002530100702.

[10] D. A. Drew, "Mathematical modeling of two-phase flow. Annual Reviews on Fluid Mechanics", *American Journal of*

Computational Mathematics, vol. 15, 1983, pp. 261–291. https://doi.org/10.1146/annurev.fl.15.010183.001401.

[11] U. K. Deb and M. I. Monir, "A computational model of microalgae culture in a TPBR for biofuel production", *The 10th International Forum on Strategic Technology*, 2015, pp. 250–253, Indonesia.

[12] I. A. Khanam and U. K. Deb, "Calculation of the average irradiance and the microalgae growth for a year at CUET, Bangladesh" *American Journal of Computational Mathematics*, vol. 6, 2016, pp. 237–244. https://doi.org/10.4236/ajcm.2016.63024.

[13] F. Akter and U. K. Deb, "Computational Modeling and Dynamics of the Oil and Water Flow Using the Galerkin Approximation", *American Journal of Computational Mathematics*, vol. 7, 2017, pp. 58–69. https://doi.org/10.4236/ajcm.2017.71005.

[14] S. Barua and U. K. Deb, "Hydrodynamics of Microalgae and CO2 flow in a Tubular Photobioreactor and consequent effects on Microalgae growth" *Rajshahi University Journal of Science and Engineering*, vol. 44, 2016, pp. 75–83.

[15] W. H. Yu and B. Wiwatanapattaphee (eds.), "Finite Element Method and Application", *Misterkopy Publishing Company*, Bangkok, 2006.

[16] A. Sayma (eds.), "Computational Fluid Dynamics", Ventus Publishing ApS, 2009.

[17] R. Kavitha and J. Angel, "Impact of Rotation and Chemical Reactions on MHD Mixed Convection Flow over an Inclined Heated Porous Plate with Heat and Mass Transfer Analysis", *WSEAS Transactions on Fluid Mechanics*, vol. 20, 2025, pp. 40-50. https://doi.org/10.37394/232013.2025.20.5.

[18] A. Omar, B. Hocine, B. Ahmed and A. Abderahim, "Experimental and CFD Investigations on Turbulent Fluid Flow Aerodynamics over Different Body Geometries", *WSEAS Transactions on Fluid Mechanics*, Vol. 20, 2025, pp. 151–161. https://doi.org/DOI: 10.37394/232013.2025.20.15.

[19] F. G. A. Fernández, J. M. F. Sevilla, J. A. S. Pérez, E. M. Grima and Y. Chisti, "Airlift-driven external-loop tubular photobioreactors for outdoor production of microalgae: assessment of design and performance", *Chemical Engineering Science*, vol. 56, 2001, pp. 2721-2732. https://doi.org/10.1016/S0009-2509(00)00521-2

[20] Q. B´echet, A. Shilton and B. Guieysse, "Modeling the effects of light and temperature on algae growth: State of the art and critical assessment for productivity prediction during outdoor cultivation", *Biotechnology Advances*, vol. 31, 2013, pp. 1648–1663. https://doi.org/10.1016/j.biotechadv.2013.08.014

[21] J. F. Andrews, "A mathematical model for the continuous culture of microorganisms utilizing inhibitory substrates", *Biotechnology and Bioengineering*, vol. X, 1968, pp. 707–723. https://doi.org/10.1002/BIT.260100602.

[22] C. N. Economou, G. Aggelis, S. Pavlou and D. V. Vayenas, "Modeling of singlecell oil production under nitrogen-limited and substrate inhibition conditions", *Biotechnology and Bioengineering*, vol. 108, 2011, no. 5, pp. 1049–1055,2011. https://doi.org/10.1002/bit.23026.

[23] J. C. Ogbonna, H. Yada and H. Tanaka, "Kinetic study on light-limited batch cultivation photosynthetic cells", *Journal of Fermentation and Bioengineering*, vol. 80, 1995, no. 3, pp. 259–264. https://doi.org/10.1016/0922-338X(95)90826-L.

[24] G.O. James, C. H. Hocart, W. Hillier, H. Chen, F. Chordbacheh, G. D. Price and M. A. Djordjevic, "Fatty acid profiling of chlamydomonas reinhardtii under nitrogen deprivation", *Bioresource Technology*, vol. 102, 2010, no. 3, pp. 3343-512010. https://doi.org/10.1016/j.biortech.2010.11.051.

[25] R. Tevatia, Y. Demirel and P. Blum, "Kinetic modeling of photoautotropic growth and neutral lipid accumulation in terms of ammonium concentration in chlamydomonas reinhardtii", *Bioresource Technology*, vol. 119, 2012, pp. 419–424. https://doi.org/10.1016/j.biortech.2012.05.124.

[26] E. M. Grima F. G. Carnacho, J. A. S. Perez, J. M. F. Sevilla, F. G. A. Fernandez and A. C. Gomez, "A mathematical model of microalgal growth in light-limited chemostat culture", *J. Chem Tech. Biotechnol*, vol. 61, 1994, pp. 167–173.

[27] Y. C. Jeon, C. W. Cho and Y. S. Yun, "Measurement of microalgal photosynthetic activity depending on light intensity and quality", *Biochemical Engineering Journal*, vol. 27, 2005, pp. 127–131. https://doi.org/10.1016/j.bej.2005.08.017.

[28] S. Aiba, "Growth kinetics of photosynthetic microorganisms", *Osaka*, pp. 85–156, 2005.

[29] D. Zhang, P. Dechatiwongse, E.A. Rio-Chanona, G.C. Maitland, K. Hellgardt and V.S. Vassilidis "Modelling of light and temperature influences on cyanobacterial growth and biohydrogen production", *Algal Research*, vol. 9, 2015, pp. 263–274. https://doi.org/10.1016/j.algal.2015.03.015

[30] M. Bekirogullari, J. Pitman, C.Theodoropoulo, "Integrated Computational and Experimental Studies of Microalgal Production of Fuels and Chemicals", *Computer Aided Chemical Engineering*, vol. 37, 2015, pp. 2393-2398. https://doi.org/10.1016/B978-0-444-63576-1.50093-5

[31] M. Bekirogullari, I. S. Fragkopoulos and J. K.Pittman, Theodoropoulos, "Production of lipid-based fuels and chemicals from microalgae: Anintegrated experimental and model-basedoptimization study", *Algal Research*, vol. 23, 2017, pp. 78-87. https://doi.org/10.1016/j.algal.2016.12.015.

[32] G. Zhao, X. Gao, C. Zhang and G. Sang, "The effects of turbulence on phytoplankton and implications for energy transfer with an integrated water quality-ecosystem model in a shallow lake", *Journal of Environmental Management*, vol. 256, 2020, pp. 1-11. https://doi.org/10.1016/j.jenvman.2019.109954.

Contribution of Individual Authors to the Creation of a Scientific Article (Ghostwriting Policy)

This research paper is collaborative work. The contribution of each author is outlined below:

Mohammad Iftekhar Monir: Developed the main idea and FEM simulation model for two-phase turbulent flow. Also conducted data analysis and interpreted the results. Prepared the manuscript.

Nurun Nahar: Assisted in developing the simulation model and data analysis, and contributed to the data collection.

Ujjwal Kumar Deb: Conceptualized the research idea and designed the FEM analysis.

Anjan Kumar Chowdhury: Supervised the research and provided guidance.

Finally, all authors reviewed and approved the final manuscript.

Sources of Funding for Research Presented in a Scientific Article or the Scientific Article Itself

Self-funding

Conflict of Interest

The authors have no conflicts of interest to declare.